standard deviations of five experiments at each temperature are given Table 1. All measurements were performed on a single composite specimen. These data may be compared with prior work over a complementary temperature range. Figure 1 shows our data for thermal conductivity along with that of Shoemaker et al.,[3] who used a laser-flash method on a pressed-powder specimen. The agreement is good. Another comparison is afforded by measurements of the specific heat using differential scanning calorimetry (DSC), also reported by Shoemaker et al. Utilizing the definition of thermal diffusivity $\alpha = \lambda/(\rho c_p)$, where α is the diffusivity, λ is the thermal conductivity, ρ is the mass density, and c_p is the specific heat, we computed a value for the specific heat from our measured values of conductivity and diffusivity. We assumed a value for the powder density of 1.716 g/cc based on 95% of TMD (1.806 g/cc)[4] mentioned above. The resulting comparison is shown in Fig. 2 along with the addition of a third set of data given by Dobratz.[4] The agreement among all three data sets is good. Shoemaker et al. state that military-grade RDX was used in their experiments. This means that up to about 20% of HMX may have existed as an impurity in their test specimens; no chemical analysis was reported by these authors. Also, no information on sample purity was given for the data quoted by Dobratz.[4]

Discussion

According to theory,[5] the intrinsic thermal conductivity of a dielectric crystalline material, i.e., the conductivity in the absence of lattice imperfections, has a $1/T$ temperature dependence at high temperatures. For this reason the data of Fig. 1 are plotted on a log-log scale, and the thin straight line is a least-squares fit of the function b/T to the combined data sets excluding the point at lowest temperature. The resulting value of b is 0.147 in the units appropriate to the figure. In the low-temperature limit, λ increases with temperature, according to theory.[5] A peak is thus expected on theoretical grounds in the curve $\lambda(T)$. The line b/T is consistent with the standard deviations of our three highest temperature measurements and the data of Shoemaker et al.[3]; however, our lowest temperature measurement is almost five standard deviations below the b/T line. We therefore speculate that our data encompasses the maximum in $\lambda(T)$ for RDX, and draw the heavy curved line in Fig. 1 to suggest a functionality consistent with all of the data. Further measurements at still lower temperatures would be desirable to confirm this behavior, but were not possible within the constraints of this work. Interestingly, the value of b obtained from a least-squares fit to the Shoemaker et al. data alone differed from the value obtained from a fit to our data alone (excluding the data at 255 K) by only 0.3%, a fact that is not immediately evident from Fig. 1, but one that adds confidence to the combined-data fit. Finally, we note that the fit, $\lambda(T) = b/T$, found above should provide a reasonable basis for extrapolation up to the melting point 478 K, provided that the application times considered do not permit appreciable thermal decomposition to occur.

References

[1]Miller, M. S., and Kotlar, A. J., "Technique for Measuring Thermal Diffusivity/Conductivity of Small Thermal-Insulator Specimens," *Review of Scientific Instruments*, Vol. 64, No. 10, 1993, pp. 2954–2960.

[2]Miller, M. S., "Step-Function Current in a Metallic Foil as a Step-Function Heat-Flux Source," *Journal of Applied Physics*, Vol. 72, No. 9, 1992, pp. 3904–3907.

[3]Shoemaker, R. L., Stark, J. A., and Taylor, R. E., "Thermophysical Properties of Propellants," *High Temperatures—High Pressures*, Vol. 17, 1985, pp. 429–435.

[4]Dobratz, B. M., "Properties of Chemical Explosives and Explosive Simulants," Lawrence Livermore Lab., UCRL-51319 REV. 1, Livermore, CA, July 1974.

[5]Klemens, P. G., "Theory of the Thermal Conductivity of Solids," *Thermal Conductivity*, edited by R. P. Tye, 1st ed., Vol. 1, Academic Press, New York, 1969, Chap. 1.

Non-Darcy Mixed Convection in a Vertical Porous Channel with Asymmetric Wall Heating

H. A. Hadim* and G. Chen†
Stevens Institute of Technology, Hoboken, New Jersey 07030

Nomenclature

C = inertia coefficient
Da = Darcy number, K/W^2
Gr^* = modified Grashof number, $(g\beta TKW)/\nu^2$ or $(g\beta q_2 KW^2)/(\nu^2 k)$
g = acceleration of gravity
h = heat transfer coefficient
K = permeability of the porous medium
k = thermal conductivity
Nu = local Nusselt number
Pe = Peclet number
Pr = Prandtl number
q = heat flux
Re = Reynolds number
r_H = ratio of wall heat fluxes, q_1/q_2
r_T = ratio of wall temperature difference, $(T_1 - T_0)/(T_2 - T_0)$
T = temperature
U = dimensionless velocity in x direction
V = dimensionless velocity in y direction
$\mathbf{V}$ = velocity vector
V_0 = uniform inlet velocity
W = channel width
X = dimensionless distance in horizontal x direction
Y = dimensionless distance in vertical y direction
β = thermal expansion coefficient of the fluid
ε = porosity
ζ = vorticity, $\partial V/\partial X - \partial U/\partial Y$
θ = dimensionless temperature, $(T - T_0)/(T_2 - T_0)$ or $(T - T_0)/(q_2 W/k)$
ν = kinematic viscosity
ψ = stream function

Introduction

RECENTLY, fundamental studies of thermal convection in fluid-saturated porous media have generated significant interest due to their diverse engineering applications, including geothermal systems, building thermal insulation, enhanced oil recovery methods, nuclear waste disposal, packed-bed chemical reactors, and solid-matrix heat exchangers. Recent comprehensive reviews of convective transport in porous media are provided by Kakac et al.[1] and Nield and Bejan.[2]

As indicated by Hadim,[3] relatively few investigations have been conducted on mixed convection in vertical porous channels, and most of them were limited to the Darcy flow regime. In the present study, a detailed numerical investigation of mixed convection in a vertical porous channel heated asymmetrically at the walls is performed with particular emphasis on the developing region. Both uniform wall temperature (UWT) and uniform wall heat flux (UHF) conditions are examined for the case when buoyancy effects are assisting the "upward" flow.

Received Oct. 18, 1993; revision received May 3, 1994; accepted for publication May 13, 1994.

*Associate Professor, Department of Mechanical Engineering.
†Graduate Research Assistant, Department of Mechanical Engineering.

Analysis

The physical model consists of a vertical porous channel bounded by two impermeable walls. The flow in the channel is assumed to be steady, laminar, incompressible, and two dimensional. The porous medium is considered to be homogeneous and isotropic and is saturated with a single-phase fluid that is in thermal equilibrium with the solid matrix. The thermophysical properties of the solid matrix and the fluid are assumed to be constant except in the body force term of the momentum equations. Considering only fibrous media, the porosity is assumed to be constant throughout the channel.[3] Viscous dissipation is neglected in the energy equation. Several previous investigators have reported that the effects of thermal dispersion are important for high Reynolds number flow,[4-6] however, in the present study, a very low Reynolds number is considered (Re = 20 at the inlet), such that the local Reynolds number remains relatively low even near the walls where the velocities are high. As reviewed by Nield and Bejan,[2] at such low Reynolds number, several reported studies revealed that the effects of thermal dispersion are negligible.

The conservation equations of mass, momentum, and energy are converted into a vorticity-stream function formulation in the usual way, and the resulting dimensionless governing equations are[3]

$$\nabla^2\psi = \zeta \tag{1}$$

$$\frac{1}{\varepsilon^2}\left(-\frac{\partial\psi}{\partial Y}\frac{\partial\zeta}{\partial X} + \frac{\partial\psi}{\partial X}\frac{\partial\zeta}{\partial Y}\right) = \frac{Gr^*}{Re^2Da}\frac{\partial\theta}{\partial X} - \frac{1}{ReDa}\zeta - \frac{C}{\sqrt{Da}}\left(\frac{\partial}{\partial X}|V|V - \frac{\partial}{\partial Y}|V|U\right) + \frac{1}{Re}\nabla^2\zeta \tag{2}$$

$$-\frac{\partial\psi}{\partial Y}\frac{\partial\theta}{\partial X} + \frac{\partial\psi}{\partial X}\frac{\partial\theta}{\partial Y} = \frac{1}{Pe}\nabla^2\theta \tag{3}$$

The boundary conditions for the problem are such that a uniform upward velocity V_0 and a uniform temperature T_0 are imposed at the channel inlet. The channel walls are maintained at either uniform temperatures T_1 and T_2 or uniform heat fluxes q_1 and q_2. The boundary conditions at the exit are obtained from the fully developed conditions. The relevant boundary conditions are given in dimensionless form as

$$\text{at } X = 0,\quad 0 < Y < \infty,\quad \zeta = \frac{\partial^2\psi}{\partial X^2}$$
$$\psi = 0,\quad \theta = r_T,\quad \frac{\partial\theta}{\partial X} = -r_H \tag{4a}$$

$$\text{at } X = 1,\quad 0 < Y < \infty,\quad \zeta = \frac{\partial^2\psi}{\partial X^2}$$
$$\psi = 1,\quad \theta = 1,\quad \frac{\partial\theta}{\partial X} = 1 \tag{4b}$$

$$\text{at } Y = 0,\quad 0 < X < 1,\quad \zeta = 9,\quad \frac{\partial\psi}{\partial X} = 1,\quad \theta = 0 \tag{4c}$$

The boundary conditions at the exit are given by the fully developed conditions[7]

$$\text{at } Y \to \infty,\quad 0 < X < 1,\quad \frac{\partial\zeta}{\partial Y} = 0,\quad \frac{\partial^2\psi}{\partial Y^2} = 0,\quad \frac{\partial^2\theta}{\partial Y^2} = 0 \tag{4d}$$

The extent of the computational domain in the y direction is chosen to be large enough in order to achieve fully developed flow at the exit. This is accomplished by performing several trial runs throughout the entire range of Da considered. Selection of the proper channel length (in the y direction) is made when the results in the entrance region do not change significantly with any further increase in channel length.

The heat transfer results are presented in terms of mean (bulk) temperature and local Nusselt number as defined in Hadim.[3]

Numerical Procedure

Equations (1–4) are transformed into algebraic, finite difference equations using the control volume formulation outlined by Gosman et al.,[8] which is described in more detail by Hadim.[3,9] The mesh size used in this analysis varied with the magnitude of Darcy number. A skewed mesh was used along both coordinates. When the buoyancy effects were significant, a fine grid was used at the channel entrance and a progressively coarser grid was used further downstream. Similarly, along the x direction, the mesh was finer near the walls and coarser in the core region. In general, a 40 × 160 mesh was used except when buoyancy effects were small in which case a 20 × 160 mesh provided sufficient accuracy. The accuracy of the numerical model was verified as discussed by Hadim.[3,9]

Results and Discussion

In order to analyze the effects of the Darcy number and asymmetric heating boundary condition on the flow and heat transfer in the channel, numerical results were obtained for the case when Gr^* = 250 and Re = 20 for both UHF and UWT conditions. All the results were obtained with Pr = 0.70, and C in Forchheimer's extension of the momentum equations was fixed at 0.55 as indicated by Hadim.[3]

Velocity and Temperature Profiles

The effects of Darcy number on the centerline velocity variation are shown in Fig. 1. As the Darcy number decreases while the modified Grashof number is kept constant, buoy-

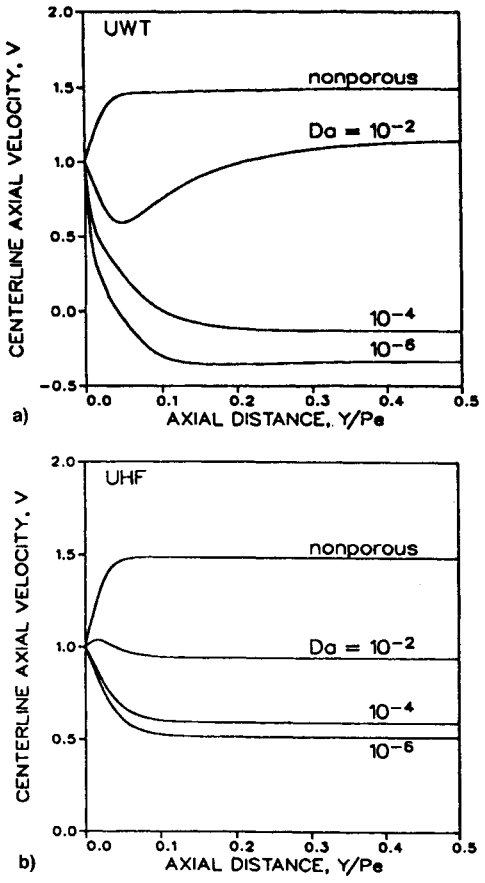

Fig. 1 Effects of Darcy number on the streamwise centerline velocity variation for Gr^* = 250, Re = 20 and a) r_T = 0.5 and b) r_H = 0.5.

ancy effects increase, which causes the velocity to increase near the walls and to decrease in the core region as explained by Hadim[7] for the symmetric heating case. For asymmetric heating, it was found that the maximum velocity occurs near the hot wall, and the distortions in the velocity profile are much sharper for the UWT condition than for the UHF condition as shown in Fig. 1. In both cases, the distortions in velocity profile increase with decreasing Darcy number. Beyond the entrance region the centerline velocity reaches an asymptotic value that decreases with decreasing Darcy number (Fig. 1). For the values of Gr^* and Re considered, it is shown in Fig. 1a that flow reversal occurs when $Da \leq 10^{-4}$. For the UHF condition, the distortions in the velocity profile are less pronounced and flow reversal did not occur (Fig. 1b).

The effect of Darcy number on the axial variation of the bulk temperature is presented in Fig. 2. For the UWT condition, the bulk temperature increases in the entrance region and reaches an asymptotic value that increases with decreasing Darcy number due to increased buoyancy effects. This is different from the symmetric isothermal heating case where the bulk temperature reached asymptotically a value of 1 for all Darcy numbers.[3] For the UHF condition, thermal energy is supplied at a constant rate such that the bulk temperature varies linearly with axial distance, and it is independent of the Darcy number as shown in Fig. 2.

Heat Transfer Results

Based on the velocity and temperature results presented so far, it is obvious that for constant modified Grashof and Reynolds numbers, the heat transfer rate increases as the Darcy number decreases as shown in Fig. 3. For the UWT condition (Fig. 3a), very close to the channel inlet, the effect of decreasing Da is important only at low values of Da as indicated by Hadim[3] for the symmetric heating case. At high Da values ($Da \geq 10^{-2}$), the flow in this region is dominated by forced convection and the Nusselt number remains constant with changing Da. Heat transfer enhancement is amplified in the mixed convection region, which exhibits a similar behavior to the symmetric heating case, but it covers a longer distance before the fully developed condition is reached. In the fully developed region, the Nusselt number reaches an asymptotic value that increases with decreasing Darcy number throughout the range of Da considered. Whereas in the symmetric heating case, the asymptotic value of the Nusselt number increases only in the non-Darcy regime, and remains virtually the same in the Darcy regime.[3] For the UHF condition (Fig. 3b) in the entrance region, small changes in the Nusselt number occur both at very high Da values ($Da \geq 10^{-2}$) as well as very low Da values ($Da \leq 10^{-4}$), and a more significant variation in the Nusselt number occurs between these two ranges. Beyond the entrance region the Nusselt number decreases gradually with increasing axial distance, but the effect of Darcy number is much less pronounced than in the UWT condition. In the fully developed region the variation of the asymptotic value of the Nusselt number is more significant at high Da values ($Da \geq 10^{-4}$).

The heat transfer results are summarized in Fig. 4, which displays the variation of the Nusselt number averaged over the entrance length of the channel with Darcy number. For both UWT and UHF conditions, the average Nusselt number exhibits a similar trend. From a high asymptotic value in the Darcy regime, the Nusselt number decreases to a lower asymptotic value when a nonporous channel condition is approached. The Darcy regime occurred at a lower Darcy number in the UWT case, and the decrease in Nusselt number is higher than in the UHF condition.

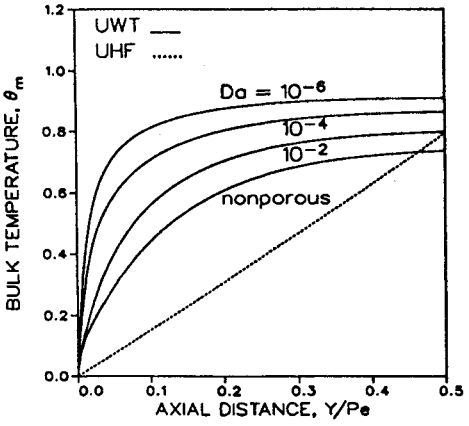

Fig. 2 Effects of Darcy number on the bulk temperature variation for $Gr^* = 250$, $Re = 20$, $r_T = 0.5$, and $r_H = 0.5$.

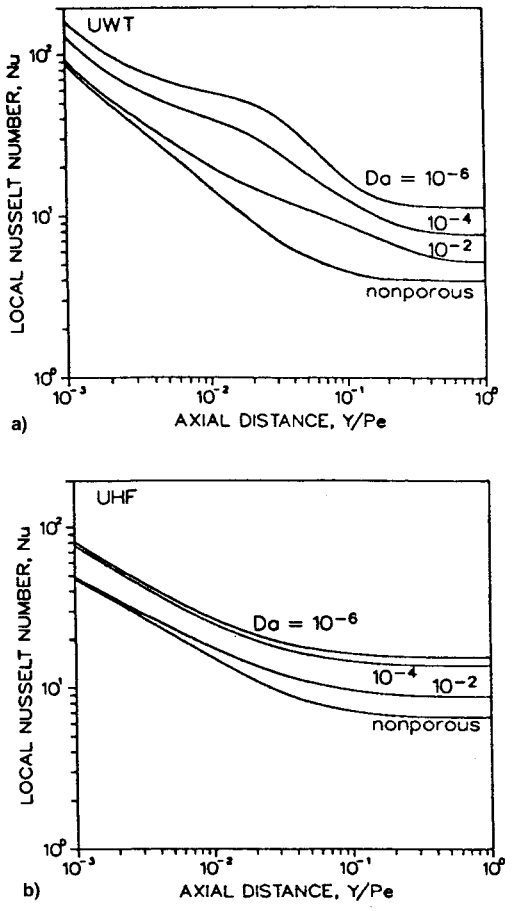

Fig. 3 Effects of Darcy number on the local Nusselt number variation for $Gr^* = 250$, $Re = 20$, and a) $r_T = 0.5$ and b) $r_H = 0.5$.

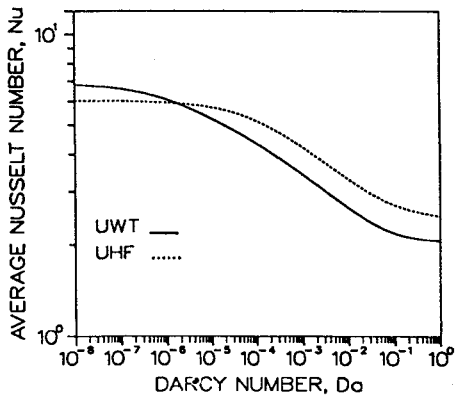

Fig. 4 Variation of average Nusselt number with Darcy number for $Gr^* = 250$, $Re = 20$, $r_T = 0.5$, and $r_H = 0.5$.

Conclusions

A numerical study of buoyancy-assisted mixed convection in a vertical porous channel with asymmetric heating at the walls was performed. The Brinkman-Forchheimer-extended Darcy model was used to account for both the inertia and the viscous effects. The evolution of mixed convection in the entrance region was examined in detail.

The results show that as the Darcy number is decreased while the modified Grashof number and the Reynolds number are kept constant, distortions in the velocity profile (which are stronger in the UWT condition), result in increased velocities near the walls leading to increased heat transfer. For the values of Gr^* and Re considered, heat transfer enhancement in the mixed convection region is more pronounced in the UWT condition. In the fully developed region, for the UWT condition, the asymptotic value of the Nusselt number increases with decreasing Darcy number throughout the entire range of Da, whereas for the UHF condition, the increase in Nusselt number was significant only at high values of Da ($Da \geq 10^{-4}$). In the UWT condition, the average Nusselt number over the entrance region decreases more steeply with Darcy number than in the UHF condition.

References

[1]Kakac, S., Kilkis, B., Kulacki, F. A., and Arinc, F., *Convective Heat and Mass Transfer in Porous Media*, Kluwer Academic, Dordrecht, The Netherlands, 1991.

[2]Nield, D. A., and Bejan, A., *Convection in Porous Media*, Springer-Verlag, New York, 1992.

[3]Hadim, A., "Numerical Study of Non-Darcy Mixed Convection in a Vertical Porous Channel," *Journal of Thermophysics and Heat Transfer*, Vol. 8, No. 2, 1994, pp. 371–373.

[4]Koch, D. L., and Brady, J. F., "The Effective Diffusivity of Fibrous Media," *AIChE Journal*, Vol. 32, No. 4, 1986, pp. 575–591.

[5]Hunt, M. L., and Tien, C. L., "Effects of Thermal Dispersion for Forced Convection in Fibrous Media," *International Journal of Heat and Mass Transfer*, Vol. 31, No. 2, 1988, pp. 301–310.

[6]Cheng, P., Chowdhury, A., and Hsu, C. T., "Forced Convection in Packed Tubes and Channels with Variable Porosity and Thermal Dispersion Effects," *Convective Heat and Mass Transfer in Porous Media*, edited by S. Kakac, B. Kilkis, F. A. Kulacki, and F. Arinc, Kluwer Academic, Dordrecht, The Netherlands, 1991, pp. 625–653.

[7]Roache, P. J., *Computational Fluid Dynamics*, Hermosa Publishers, Albuquerque, NM, 1982.

[8]Gosman, A. D., Pun, W. M., Runchal, A. K., Spalding, D. B., and Wolfshtein, M., *Heat and Mass Transfer in Recirculating Flows*, Academic Press, New York, 1969.

[9]Hadim, A., "Forced Convection in a Porous Channel with Localized Heat Sources," *Journal of Heat Transfer*, Vol. 116, No. 2, 1994, pp. 465–472.

Wideband Spectral Models for the Absorption Coefficient of Water Vapor

Kouichi Kamiuto* and Yuji Tokita†
Oita University, Oita 870-11, Japan

Introduction

THE exponential wideband model developed by Edwards and Menard[1] has been utilized successfully to solve many radiative transfer problems in high-temperature systems, but it is well recognized that this model does not take into account the effect of nonblack walls in radiative transfer calculations.[2] This deficiency may be readily overcome if spectral computations are performed utilizing an appropriate wideband spectral model for the absorption coefficients of participating gases. Desoto and Edwards[3] and Edwards et al.[4] proposed such a spectral model on the basis of the exponential wideband model, and made use of this model to analyze radiative transfer in nonisothermal and nongray gases, but this wideband spectral absorption coefficient was assumed to be only applicable to the overlapped-line case. Recently, another exponential band-envelope model was utilized by Taniguti et al.[5] to solve a radiative equilibrium problem in nongray gases. This model, however, possesses a defect. The calculated total emissivity of an isothermal gas is systematically underpredicted because of the presence of $\tanh(2\eta)$, where η denotes the line overlap parameter, in the expression for the absorption coefficient.

The present study aims at improving these wideband spectral models for infrared gases, particularly water vapor. First, additional parameters are introduced into the above-mentioned spectral models, and then optimally adjusted at various total and partial gas pressures utilizing a least-squares method. Finally, a comparison between two wideband spectral models with optimally adjusted free parameters is made with respect to the total emissivity of an isothermal water vapor layer.

Received Dec. 7, 1993; revision received March 17, 1994; accepted for publication May 9, 1994.

*Professor, Department of Production Systems Engineering. Member AIAA.

†Professor, Department of Production Systems Engineering.

Wideband Spectral Models

Edwards et al.[4] proposed the following wideband spectral model for the absorption coefficient of an infrared gas at high pressures or at high temperatures:

$$\kappa_\nu^{(1)} = (\alpha/K_1\omega)\exp(-\Delta\nu/K_1\omega) \tag{1}$$

where α is the integrated band intensity ($\mathrm{cm}^{-1}/\mathrm{gm}^{-2}$), ω is the bandwidth parameter (cm^{-1}) and K_1 is a numerical factor assumed to be 1.0.[4] Furthermore, $\Delta\nu$ is defined as follows: $\Delta\nu = \nu_u - \nu$, for an asymmetric band with upper limit ν_u, $\Delta\nu = \nu - \nu_l$, for an asymmetric band with lower limit ν_l, and $\Delta\nu = 2|\nu - \nu_c|$, for a symmetric band with center ν_c. In the expressions for $\Delta\nu$, ν is the wave number of radiation. As shown later, this model can be utilized with an acceptable accuracy even for nonoverlapped-line cases by appropriately adjusting a value of K_1.

In addition to the above Edwards model, another exponential band-envelope model,[5] which is called the modified Edwards model in the present study, was derived by neglecting the cosine term appearing in Elsasser's band model. The absorption coefficient based on this model is written as

$$\kappa_\nu^{(2)} = (\alpha/\omega)\exp(-\Delta\nu/\omega)\tanh(K_2\eta) \tag{2}$$

where K_2 is a numerical factor equal to 2.5 Unfortunately, as pointed out earlier, this model underestimates the absorption in comparison with Eq. (1), unless the value of K_2 is increased.

As readily found, when $K_2 \to \infty$, the modified Edwards model is reduced to the Edwards model with $K_1 = 1$, which may be obtained by averaging Elsasser's regular band model with the exponential band-envelope over a mean line spacing d, because

$$\kappa_\nu = \frac{1}{d}\int_{-d/2}^{d/2} \frac{(\alpha/\omega)\exp(-\Delta\nu/\omega)\sinh(2\eta)}{\cosh(2\eta) - \cos(2\pi\nu^*/d)}\,\mathrm{d}\nu^* = (\alpha/\omega)\exp(-\Delta\nu/\omega) \tag{3}$$

Optimizations of K_1 and K_2

In order to utilize the above-mentioned wideband spectral models under various gas temperatures and pressures, two